ACS Medicinal Chemistry Letters

pubs.acs.org/acsmedchemlett Letter

Dissecting Polypharmacology in Phenotypic Screening to Resolve Ferroptotic and Necrotic Cell-Death Mechanisms

Kenichi Shimada,* Elisabet Gregori-Puigjane, Michael E. Stokes, Rachid Skouta, and Brent R. Stockwell*

Cite This: https://doi.org/10.1021/acsmedchemlett.6c00020 Read Online

ACCESS | Metrics & More | Article Recommendations | Supporting Information

ABSTRACT: Small molecules frequently induce heterogeneous cell-death programs, complicating the mechanistic interpretation and optimization. Here, we investigate the ferroptotic and necrotic activities of the lethal small molecule CIL56 and related analogs. Although structurally similar, these compounds induce chemically separable death phenotypes. A phenotypic suppressor screen further identified distinct sets of small molecules that selectively attenuate ferroptotic or necrotic death. Classification of suppressor compounds based on shared ligand-based target predictions suggested nonoverlapping groups of candidate protein targets linked to each death modality. Together, these results show that integrating phenotypic screening with suppressor classification and target prediction can improve the interpretability of small-molecule phenotypic screens by prioritizing candidate proteins and pathways underlying the observed biological response.

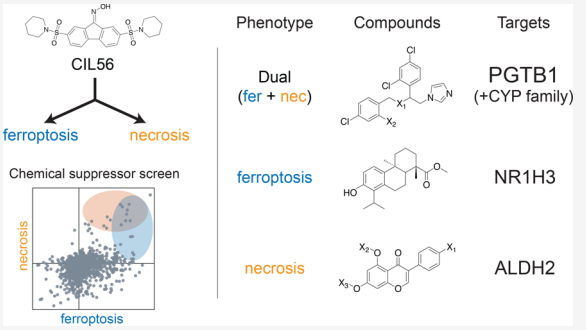

KEYWORDS: *polypharmacology, phenotypic cell-based screening, chemical annotation, nonapoptotic cell death, ferroptosis, similarity ensemble approach*

INTRODUCTION

Phenotypic screening has played a central role in the discovery of small-molecule modulators of complex biological processes,[1] particularly in cases where molecular targets are unknown or polypharmacology is intrinsic to efficacy. However, a persistent challenge of phenotypic screening is that individual compounds frequently engage multiple targets and pathways, giving rise to phenotypic outcomes that can be achieved through distinct underlying biological programs, thereby complicating mechanistic interpretation and downstream medicinal chemistry optimization.[2,3]

Cell death represents a particularly tractable and biologically important context in which this challenge becomes explicit because similar lethal phenotypes can arise from mechanistically distinct programs.

Ferroptosis is a regulated, iron-dependent form of nonapoptotic cell death characterized by lipid peroxidation and sensitivity to radical-trapping antioxidants such as α-tocopherol.[4] In contrast, nonferroptotic, necrotic cell death encompasses ferroptosis-independent processes that are often less well-defined at the molecular level. Small molecules capable of engaging both ferroptotic and necrotic pathways provide useful probes for dissecting these modalities but also highlight the difficulty of assigning a mechanism based solely on lethality or single-condition assays.

CIL56 is a lethal small molecule previously shown to induce cell death through mechanisms related to lipid peroxidation, yet evidence suggests that its activity cannot be explained by a single death pathway.[5,6] Subsequent studies have shown that CIL56 induces a nonapoptotic, lipid-associated form of cell death that is genetically and phenotypically distinct from canonical ferroptosis or necroptosis, implicating broader disruption of lipid homeostasis and membrane-associated processes rather than a single regulated death.[7−9] Structurally related analogs of CIL56 provide an opportunity to examine how subtle chemical differences influence death modality and to determine whether ferroptotic and necrotic components can be functionally separated. In parallel, systematic identification of small-molecule suppressors offers a complementary strategy to interrogate the pathways that modulate these phenotypes.

Here, we investigate the ferroptotic and necrotic activities of CIL56 and related analogs using a phenotypic suppressor screening approach. By combining condition-specific screening with ligand-based target prediction, we aim to improve the interpretability of small-molecule−induced death phenotypes and to prioritize candidate proteins and pathways underlying distinct cell-death modalities relevant to medicinal chemistry optimization.

Received: January 8, 2026
Revised: March 13, 2026
Accepted: March 17, 2026

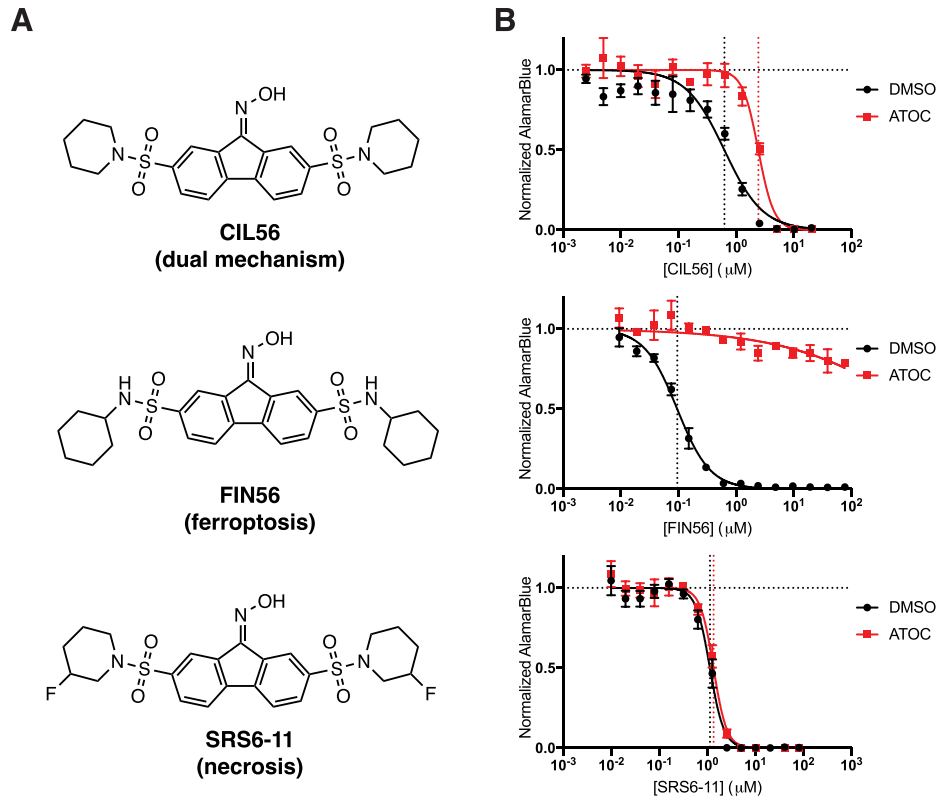

Figure 1. Chemical bifurcation of CIL56-induced cell death. (A) Chemical structures of CIL56 and two analogs, FIN56 and SRS6−11. (B) Dose−response viability curves of CIL56, FIN56, and SRS6−11 in HT-1080 cells in the presence of vehicle (DMSO) or the ferroptosis inhibitor α-tocopherol (ATOC, 100 μM).

RESULTS AND DISCUSSION

Chemical Bifurcation of CIL56-Induced Cell Death

To examine whether structurally related compounds induce distinct cell-death phenotypes, we first compared the activity of CIL56 with two closely related analogs, FIN56 and SRS6−11 (Figure 1A).[5,6] Although these compounds share a common chemical scaffold, prior observations suggested that their lethal activities may not be mechanistically equivalent. We therefore assessed their effects on cell viability under conditions designed to distinguish ferroptotic and nonferroptotic death modalities.

Dose−response analyses in HT-1080 cells revealed marked differences in the sensitivity of compound-induced lethality to the radical-trapping antioxidant α-tocopherol (ATOC) (Figure 1B).[4] FIN56-induced cell death was strongly suppressed by ATOC across the tested concentration range, consistent with a ferroptosis-dominant phenotype. In contrast, SRS6−11 retained substantial lethality in the presence of ATOC, indicating a ferroptosis-independent necrotic cell-death component. CIL56 exhibited intermediate behavior, with partial suppression by ATOC at lower concentrations and persistent lethality at higher concentrations, suggesting the coexistence of ferroptotic and necrotic death components.

These results demonstrate that subtle chemical differences among CIL56-related compounds are sufficient to bias cell death toward distinct phenotypic modalities. These phenotypic differences are consistent with prior structure−activity relationship (SAR) analysis of CIL56 analogs, in which systematic modifications of the oxime functionality and sulfonamide-linked amine substituents altered sensitivity to the radical-trapping antioxidant α-tocopherol.[5] In that study, FIN56 (SRS7−34) exhibited marked α-tocopherol rescue (>160-fold selectivity), whereas analogs such as SRS6−11 showed minimal rescue. These findings indicate that relatively subtle structural perturbations within the CIL56 scaffold can substantially shift the balance between ferroptosis-sensitive and ferroptosis-independent death components. In the present work, we reinterpret differential α-tocopherol rescue within a modality-separation framework, demonstrating that these SAR-driven differences correspond to biasing of ferroptotic versus necrotic execution programs. Importantly, this chemical bifurcation establishes a tractable experimental system in which ferroptotic and necrotic components of cell death can be functionally separated, providing a foundation for subsequent phenotypic suppressor screening and mechanistic prioritization.

Closely related compounds display distinct sensitivities to α-tocopherol, revealing ferroptosis- and necrosis-dominant death phenotypes.

Phenotypic Suppressor Screening Resolves Ferroptotic versus Necrotic Modulation

To investigate the mechanisms underlying CIL56-induced cell death, we performed a phenotypic enhancer and suppressor screen in HT-1080 cells under conditions that functionally separated the ferroptotic and necrotic components. Because CIL56 induces both phenotypes in a concentration-dependent manner, direct screening using this compound alone risks conflating mechanistically distinct death modalities.

Although structurally related analogs that selectively induce ferroptosis or necrosis were identified subsequently, these compounds were not available at the time of screening. We

https://doi.org/10.1021/acsmedchemlett.6c00020
ACS Med. Chem. Lett. XXXX, XXX, XXX−XXX

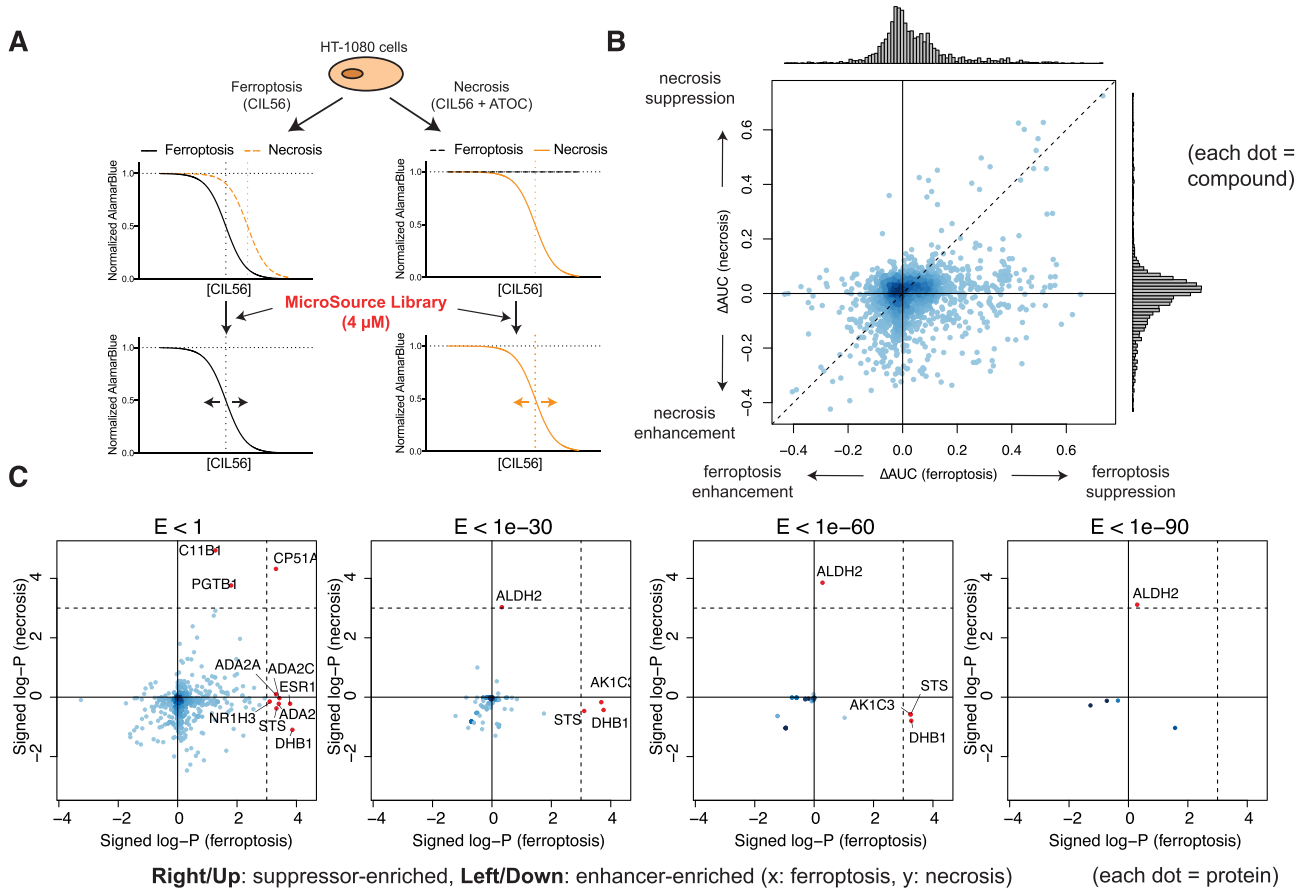

Figure 2. Phenotypic suppressor screening resolves ferroptotic versus necrotic modulation HT-1080 cells were cotreated with CIL56 under conditions favoring ferroptosis or necrosis in the presence of nontoxic MicroSource library compounds. (A) Schematic illustrating phenotypic separation of CIL56-induced cell death. CIL56 alone induces ferroptosis-dominant death, whereas cotreatment with α-tocopherol suppresses the ferroptotic component, revealing a necrotic phenotype at higher CIL56 concentrations. (B) Summary of the enhancer/suppressor screen. Changes in area under the dose−response curve (ΔAUC) upon modulator treatment are plotted for ferroptosis (x-axis) and necrosis (y-axis). (C) Directional summary of target enrichment results across representative Similarity Ensemble Approach E-value thresholds, highlighting consistent suppressor and enhancer trends.

therefore implemented a pharmacological separation strategy using CIL56 in the presence or absence of α-tocopherol (ATOC) to bias death outcomes toward specific modalities. Under ferroptosis-favoring conditions, HT-1080 cells were treated with CIL56 at concentrations ranging from 0.31 to 1.25 μM, where necrotic death was minimal (Figure 1B). To isolate a necrotic phenotype, cells were cotreated with higher concentrations of CIL56 (1.25 or 2.5 μM) and ATOC (100 μM), which suppresses ferroptosis and unmasks ferroptosis-independent lethality (Figure 2A).

Prior to suppressor analysis, the intrinsic cytotoxicity of the MicroSource library was assessed. HT-1080 cells were treated with library compounds (0.5−4 μM) in the presence or absence of ATOC for 48 h. Of the 1,841 compounds tested, 1,671 were nonlethal and were retained as candidate modulators (Figure S1A). Among the excluded compounds, a small subset exhibited ATOC-sensitive lethality, consistent with ferroptosis-like activity (Figure S1B), and were not considered further.

For suppressor screening, HT-1080 cells were cotreated with individual modulators (4 μM) and either CIL56 alone or CIL56 plus ATOC. CIL56 was applied as a 2- or 3-point 2-fold dilution series, and cell viability was measured after 48 h. Modulator effects were quantified as the change in area under the dose−response curve (ΔAUC) relative to DMSO controls, enabling direct comparison of modulatory effects across ferroptotic and necrotic death modalities (Figure 2B). Complete screening results for all library compounds are provided in Supporting Information 1.

While the resulting ΔAUC landscape revealed a clear structure in how small molecules modulated ferroptotic and necrotic death, interpretation at the level of individual compounds remained challenging. To obtain a higher-level, target-centric view of phenotype-specific modulation, we aggregated screening outcomes using Target Enrichment Analysis (TEA), a ligand-based framework that integrates phenotypic screening data with predicted protein−compound associations derived from the Similarity Ensemble Approach (SEA) (schematized in Figure S2; see Experimental Section and Supporting Methods).[10−12]

A practical limitation of ligand-based target prediction in phenotypic screening contexts is that confidence thresholds for compound−target assignments (e.g., SEA E-values) do not have a universally established optimum for phenotypic screening data sets, and prediction stringency can influence downstream interpretation. We therefore examined how predicted target assignments and enrichment results varied across a range of SEA E-value cutoffs (Figure S3). To ensure

https://doi.org/10.1021/acsmedchemlett.6c00020
ACS Med. Chem. Lett. XXXX, XXX, XXX−XXX

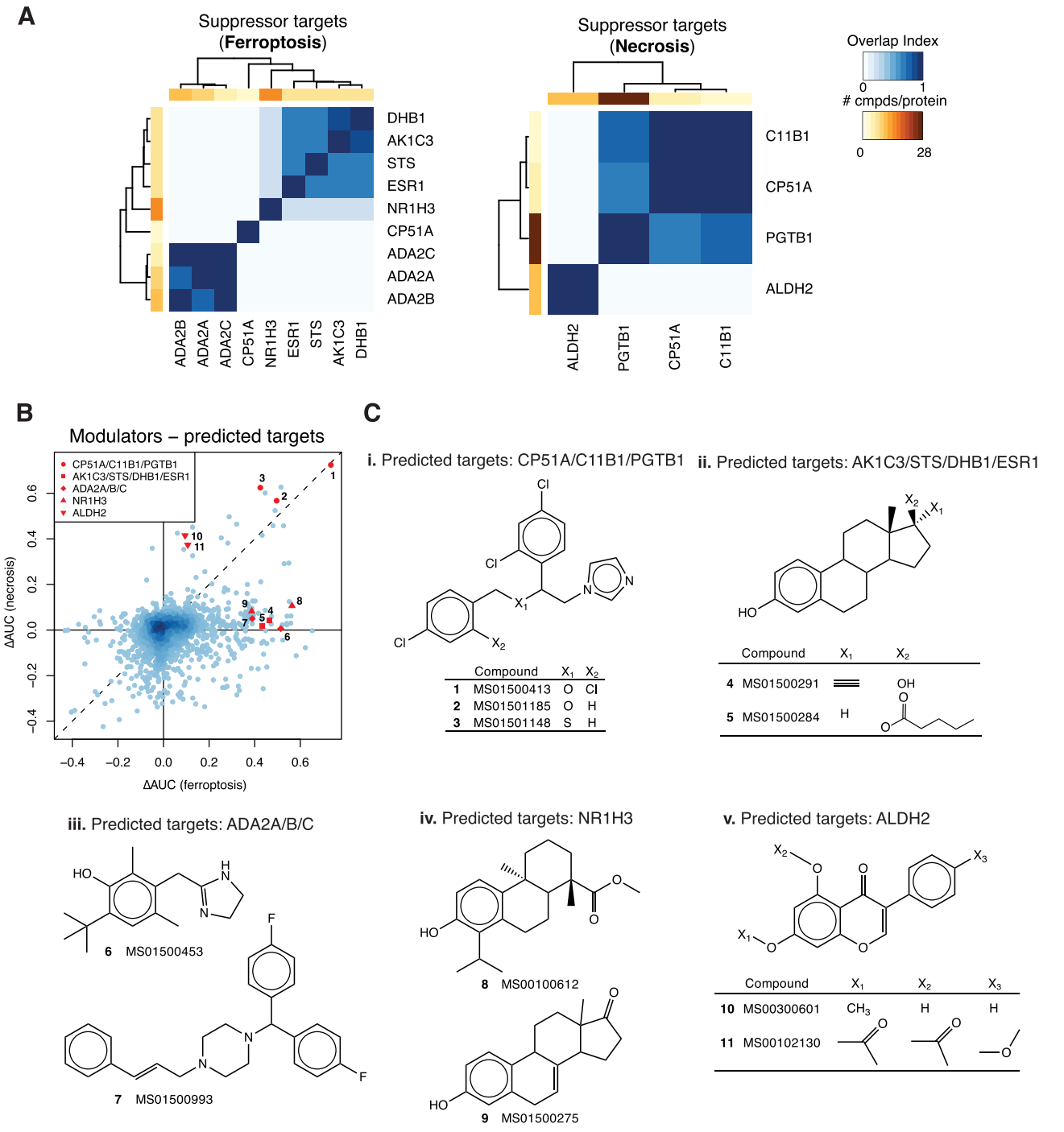

Figure 3. Suppressor chemotypes define distinct mechanistic classes. (A) Overlap analysis of leading-edge compounds across predicted protein targets reveals nonoverlapping suppressor classes for ferroptosis and necrosis. (B) Phenotypic distribution of suppressor compounds from the screening data set (same coordinates as Figure 2B), with distinct chemotypes highlighted. (C) Representative suppressor compounds and their predicted protein targets, illustrating chemically separable classes associated with modulation of ferroptotic or necrotic cell death.

that mechanistic prioritization was not driven by an arbitrary threshold choice, enrichment analyses were repeated across multiple confidence levels and enrichment patterns among suppressor and enhancer sets were compared under each cutoff (Figure S4). Predicted ligand−target associations for all screening compounds are provided in Supplemental Data 2.

Using representative confidence thresholds informed by these sensitivity analyses, target enrichment results were summarized in Figure 2C. Enrichment trends were consistent across multiple E-value cutoffs, highlighting candidate target classes preferentially associated with suppression of either ferroptotic or necrotic death. Importantly, these trends reflected collective behavior across compound sets rather than isolated outliers, establishing a robust target-centric summary of phenotype-specific modulation. Full target enrichment results across all confidence thresholds are provided in Supplemental Data 3.

Target Enrichment and Overlap Analysis Reveal Distinct Suppressor Classes. Having summarized phenotype-specific target enrichment trends (Figure 2C), we next

https://doi.org/10.1021/acsmedchemlett.6c00020
ACS Med. Chem. Lett. XXXX, XXX, XXX−XXX

asked whether suppressors of CIL56-induced ferroptotic and necrotic cell death could be organized into distinct chemical and predicted target classes. To address this, we examined protein targets that were significantly enriched among suppressors or enhancers at representative SEA confidence thresholds and compared the sets of active compounds contributing to each enrichment signal.

Analysis of compound-set overlap revealed a clear structure among enriched protein targets (Figure 3A). Some targets were supported by highly overlapping groups of suppressor compounds, whereas others were associated with largely distinct compound subsets, indicating the presence of multiple, separable suppressor classes. Notably, targets preferentially enriched among ferroptosis suppressors tended to group separately from those enriched among necrosis suppressors, suggesting that modulation of these two death modalities is associated with distinct predicted target landscapes. This separation was further reflected at the compound level, where suppressor classes associated with ferroptotic or necrotic modulation exhibited distinct patterns of activity across the two death modalities (Figure S5).

To visualize these relationships in the context of the original phenotypic screen, we overlaid enriched suppressor classes onto the ΔAUC landscape (Figure 3B). Compounds associated with different predicted target classes localized to distinct regions of the ferroptosis−necrosis modulation space, consistent with phenotype-specific suppression rather than nonspecific cytoprotection. Importantly, compounds predicted to target proteins within the same overlap-defined class exhibited similar modulation profiles, reinforcing the internal consistency of the classification.

Representative chemical structures and predicted protein targets corresponding to each suppressor class are shown in Figure 3C. These classes encompass chemically diverse scaffolds predicted to engage nonoverlapping sets of protein targets, underscoring the ability of phenotypic suppressor screening combined with ligand-based target enrichment to resolve heterogeneous cell-death mechanisms at a systems level. Importantly, TEA does not imply that all proteins associated with a given suppressor class must be simultaneously perturbed to achieve phenotypic suppression. Rather, the enrichment reflects that suppressor compounds within a class are predicted to engage one or more proteins from the same target set, any subset of which may be sufficient to attenuate the corresponding cell-death program. Thus, the convergence of phenotypic modulation, target enrichment, and compound overlap provides a focused, biologically interpretable set of hypotheses—prioritizing candidate proteins and pathways for subsequent mechanistic validation.

Integrating suppressor profiling across five compound classes reveals a structured organization of the CIL56-modulating pathways (Figure 3C). Class I suppressors are the most informative, identifying PGTB1, CP51A, and C11B1 (HGNC symbols: PGGT1B, CYP51A1, and CYP11B1) as targets that converge on lipid and membrane regulatory processes and produce the strongest suppression across both cell death phenotypes. Among these, PGTB1 is particularly notable, as it regulates prenylation-dependent membrane targeting of signaling and trafficking proteins, a foundational step that often precedes and cooperates with other lipid modifications to stabilize proteins at Golgi and plasma membranes.[13,14] Perturbation of prenylation therefore implicates membrane anchoring and organization as upstream determinants of CIL56 sensitivity. Consistent with this view, prior screens identified ZDHHC5/GOLGA7-dependent palmitoylation as a strong suppressor of CIL56-induced cell death, without resolving the specific death modality involved.[7−9] Together with our findings, these results suggest that disruption of membrane-anchoring machinery—via either prenylation or palmitoylation—suppresses both ferroptotic and nonferroptotic components of CIL56-induced lethality, rather than selectively targeting a single death execution pathway.

In contrast to this upstream membrane-organizing layer, the remaining suppressor classes map more directly to death-modality−biased components of CIL56 lethality. Classes II−IV predominantly align with the ferroptotic component by modulating the lipid-peroxidation susceptibility rather than directly targeting downstream death-execution machinery. Class II targets (AK1C3, STS, DHB1; HGNC symbols: AKR1C3, STS, and HSD17B1) encode redox-active enzymes involved in steroid and sterol metabolism that shape membrane composition, lipid-peroxidation pressure, and the handling of reactive lipid-derived species.[15−17] Consistent with this framework, inhibition of sterol metabolism and related redox enzymes has been reported to suppress ferroptotic cell death.[5,18] Class III targets (ADA2A/B/C; HGNC symbols: ADRA2A, ADRA2B, ADRA2C) are best interpreted as metabolic context modifiers that indirectly influence lipid-peroxidation sensitivity,[19,20] while Class IV highlights NR1H3 as a transcriptional regulator of cholesterol and phospholipid homeostasis that tunes membrane vulnerability to lipid oxidation.[21] By contrast, Class V uniquely maps to a necrotic axis, with ALDH2 limiting the accumulation of reactive lipid-derived aldehydes that can destabilize membrane-associated protein networks.[22,23] Together, these patterns support a model in which CIL56 integrates a FIN56-like ferroptotic program with additional membrane- and aldehyde-driven necrotic processes, conditioned by upstream regulation of membrane anchoring and lipid organization.

CONCLUSION

In this study, we demonstrate that closely related small molecules can induce distinct ferroptotic and necrotic cell-death phenotypes and that phenotypic suppressor screening can be used to functionally separate and interrogate these modalities. By integrating phenotype-specific screening outcomes with ligand-based target prediction using SEA and Target Enrichment Analysis, we established a systematic approach to prioritize candidate protein targets and suppressor classes associated with heterogeneous cell-death responses. While TEA identifies protein targets statistically associated with phenotypically active compound sets rather than causally required mechanisms, ligand-based prediction using SEA is inherently dependent on the scope and quality of available reference ligand databases, may yield false-positive associations, and does not provide direct evidence of physical target engagement. Accordingly, SEA was used here as a hypothesis-generating prioritization tool rather than a definitive target assignment. Definitive mechanistic assignment will therefore require orthogonal validation, including testing selective inhibitors of prioritized predicted targets for shared suppressor activity or applying targeted genetic perturbation approaches. Such studies represent a focused and important direction for future investigation. Despite these considerations, the combination of phenotypic screening and target enrichment provides a rapid, inexpensive, and flexible strategy to improve the

https://doi.org/10.1021/acsmedchemlett.6c00020
ACS Med. Chem. Lett. XXXX, XXX, XXX−XXX

Scheme 1. Total Synthesis of SRS6-11

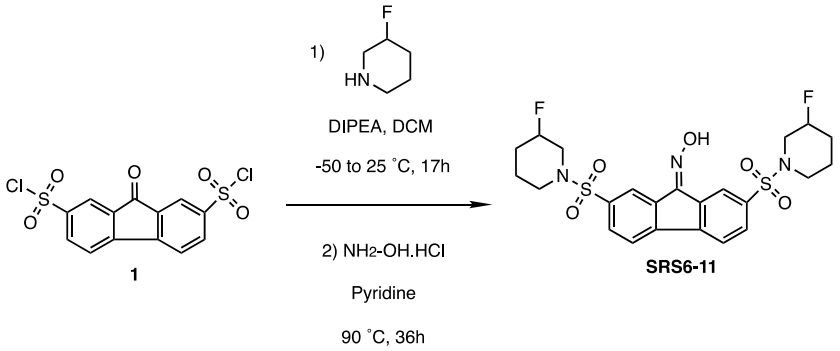

interpretability of small-molecule phenotypes and to guide focused mechanistic and medicinal chemistry follow-up.

EXPERIMENTAL SECTION

Chemical Lethality Testing in HT-1080 Cells

HT-1080 fibrosarcoma cells were purchased from the American Type Culture Collection. HT-1080 cells were grown in DMEM High-Glucose media with 1% nonessential amino acids (Thermo Fisher Scientific) and 10% FBS at 37 °C under 5% CO_2. In testing chemical lethality, we seeded 1,000 HT-1080 cells in each well of 384 well plates and immediately cotreated them with a lethal compound (CIL56, FIN56, or SRS6−11) alone or together with 100 μM α-tocopherol (ATOC). Cells were incubated for 48 h before adding AlamarBlue (Thermo Fisher Scientific) and fluorescence (488/535) was measured on a Victor3 plate reader (PerkinElmer). Dose−response curves were plotted using Prism 7 (GraphPad).

Chemical Library Screening

We used 2,000 compounds purchased from MicroSource Discovery Systems for screening. We first tested the lethality of these compounds. ATOC (100 μM) or vehicle (0.1% ethanol) was added to the HT-1080 cell suspension. The cells were seeded in 384 well plates at 1,000 cells per well. Cells were treated with 2-fold dilution series ranging from 0.5 to 4 μM and incubated for 48 h before the viability was measured using AlamarBlue. Viability was normalized using the following equation: $V_{M,X} = (I_{M,X} - I_{bg(M))}/(I_{D,X} - I_{bg(D))}$, where $V_{M,X}$ is the normalized viability of HT-1080 cells cotreated with a modulator M and X (either ATOC or vehicle), $I_{M,X}$, $I_{D,X}$, $I_{bg(M)}$, $I_{bg(D)}$ are raw Alamar blue intensity of cells treated with M and X, that treated with DMSO and X, background intensity from media and M, and background intensity from media and DMSO, respectively. We discarded 159 compounds that we failed to collect the data, but measured $V_{M,ethanol}$ and $V_{M,ATOC}$ for the other 1,841 modulators.

Next, we seeded HT-1080 cells treated with either ethanol or ATOC into 384 well plates. 1,841 different potential cell death modulators (the Microsource Collection) were further added to the plates at 4 μM. After one h, three concentrations of CIL56 (0.31, 0.62, 1.25 μM) were added to ethanol-treated HT-1080 cells to induce ferroptosis, or two concentrations of CIL56 (1.25, 2.5 μM) were added to ATOC-treated HT-1080 cells to induce necrosis. The cells were incubated for 48 h before the viability is measured using AlamarBlue. Normalized viability was measured by $V_{L,M,X} = (I_{L,M,X} - I_{bg(M))}/(I_{D,M,X} - I_{bg(M))}$, where $V_{L,M,X}$ is the normalized viability after treated with L (different concentrations of CIL56), M (modulator at 4 μM), X (vehicle or ATOC). $I_{L,M,X}$, $I_{D,M,X}$, $I_{bg(M)}$ are raw alamarBlue intensities from the cells treated with L, M, X, the cells treated with D, M, X, background intensity from media and M, respectively. To assess the effect of modulator on perturbing CIL56-induced ferroptosis or necrosis, we first computed the area under the dose−response curve (AUC) from the 3- or 2-point 2-fold dilution series of CIL56 treatment for each M and X treatments, and measured the difference, $\Delta AUC_{M,X} = AUC_{M,X} - AUC_{D,X}$.

Total Synthesis of a CIL56 Analog SRS6−11

CIL56 and FIN56 were synthesized as described previously (Nat Chem Biol. 2016 Jul;12(7):497−503. PMCID: PMC4920070). The synthesis of compound SRS6−11 was carried out following procedures based on the same report publication. The total synthesis of SRS6−11 is depicted in Scheme 1.

General Procedure for the Synthesis of 2,7-Bis(3-difluoropiperidin-1-ylsulfonyl)-9*H*-fluoren-9-one oxime (SRS6−11)

9-Oxo-9*H*-fluorene-2,7-disulfonyl dichloride (**1**) (64 mg, 0.170 mmol,1 equiv) was dissolved in 50 mL of dichloromethane and the mixture was cooled to −50 °C. To this mixture was added 3-fluoropiperidine hydrochloride (61.7 mg, 0.442 mmol, 2.6 equiv) and diisopropylethylamine (88.8 μL, 0.510 mmol, 3 equiv). The reaction mixture was stirred at room temperature for 17h. The solvent was evaporated, and the residue was purified by flash-column chromatography on silica gel to provide the desired ketone intermediate compound that was directly mixed with hydroxylamine hydrochloride (10 equiv) in pyridine (10 mL). The mixture was stirred at 95 °C for 36 h. The pyridine was evaporated, and the residue was stirred with 1 N HCl (10 mL) for several minutes and washed several times with cold water and ethanol. White product was collected by filtration to give the desired 2,7-bis(3-difluoropiperidin-1-ylsulfonyl)-9*H*-fluoren-9-one oxime (SRS6−11, 54 mg, 61%). ^{1}H NMR (400 MHz, DMSO) δ 13.35 (s, 1H), 8.67 (d, J = 1.7 Hz, 1H), 8.35 (d, J = 8.0 Hz, 1H), 8.31 (d, J = 8.0 Hz, 1H), 7.99 (dd, J = 8.5, 1.7 Hz, 2H), 7.91 (dd, J = 8.1, 1.7 Hz, 1H), 4.84 (s, 1H), 4.73 (s, 1H), 3.45 (d, J = 11.0 Hz, 2H), 3.3 (d, J = 11.0 Hz, 2H), 2.99 (d, J = 12.5 Hz, 1H), 2.96 − 2.87 (m, 1H), 2.71 (t, J = 10.5 Hz, 2H), 1.70 (d, J = 11.2 Hz, 6H), 1.55 (d, J = 12.1 Hz, 2H); MS (APCI+, M+1) 526.16.

Ligand-Based Target Aggregation and Enrichment Analysis

Ligand-based target prediction was performed using SEA,[7] which compares screening compounds to reference ligand sets derived from chemical library screening experiments curated in ChEMBL.[24] Reference compounds associated with orthologous eukaryotic protein targets were merged and clustered using Ward's hierarchical clustering method.[25] Structural similarity between screening compounds and reference ligands was quantified using extended-connectivity fingerprints (ECFP4)[26] and pairwise Tanimoto coefficients. For each ligand−target association, SEA computes an expectation value (E-value) that estimates the probability of observing the measured similarity by chance, using a statistical framework analogous to that employed by BLAST.[27]

Predicted ligand−target associations were aggregated at the protein level and analyzed using a target enrichment framework conceptually analogous to Gene Set Enrichment Analysis. Screening compounds were ranked based on their effects on CIL56-induced ferroptotic or necrotic cell death, quantified as changes in area under the dose−response curve (ΔAUC). Enrichment of predicted protein targets among suppressors or enhancers was assessed using a Kolmogorov−Smirnov-based statistic.[28] Protein targets were considered to be

https://doi.org/10.1021/acsmedchemlett.6c00020
ACS Med. Chem. Lett. XXXX, XXX, XXX−XXX

significantly enriched if they exceeded a predefined significance threshold in at least one enrichment analysis. Full parameter settings, robustness analyses, and overlap calculations are provided in the Supporting Information.

■ ASSOCIATED CONTENT

Data Availability Statement

Codes used in this study are available from https://github.com/kenichi-shimada/TEA.

Supporting Information

The Supporting Information is available free of charge at https://pubs.acs.org/doi/10.1021/acsmedchemlett.6c00020.

Methods and Figures describing Target Enrichment Analysis workflow, SEA-based ligand−target prediction, threshold sensitivity analyses, and compound class overlap analysis (PDF)

Supplemental Data 2, complete phenotypic screening results (XLSX)

Supplemental Data 3, predicted ligand−target associations (XLSX)

Supplemental Data 4, target enrichment results across SEA confidence thresholds (XLSX)

■ AUTHOR INFORMATION

Corresponding Authors

Brent R. Stockwell − *Department of Biological Sciences, Columbia University, New York, New York 10027, United States; Department of Chemistry, Department of Pathology and Cell Biology, Herbert Irving Comprehensive Cancer Center, Digestive and Liver Disease Research Center, Irving Institute for Cancer Dynamic, Columbia University, New York, New York 10027, United States;* orcid.org/0000-0002-3532-3868; Email: bstockwell@columbia.edu

Kenichi Shimada − *Department of Biological Sciences, Columbia University, New York, New York 10027, United States; Laboratory of Systems Pharmacology, Harvard Medical School, Boston, Massachusetts 02115, United States;* Email: ks2474@columbia.edu

Authors

Elisabet Gregori-Puigjane − *Department of Pharmaceutical Chemistry, University of California, San Francisco, California 94158, United States; Chemotargets SL, 08028 Barcelona, Spain*

Michael E. Stokes − *Department of Biological Sciences, Columbia University, New York, New York 10027, United States*

Rachid Skouta − *Departments of Biology and Chemistry, University of Massachusetts, Amherst, Massachusetts 01003, United States*

Complete contact information is available at: https://pubs.acs.org/10.1021/acsmedchemlett.6c00020

Author Contributions

K.S. and B.R.S. conceived of the project, designed the experiments, analyzed the data and wrote the manuscript. E.G.P. performed target prediction of MicroSource library compounds using Similarity Ensemble Approach. K.S. performed the compound screening and Target Enrichment Analysis. M.S. participated in cell culture works including compound library screening. R.S. synthesized CIL56, FIN56, and SRS6−11.

Notes

Safety Statement: No unexpected or unusually high safety hazards were encountered.

The authors declare the following competing financial interest(s): B.R.S. is an inventor on patents and patent applications involving ferroptosis, holds equity in and serves as a consultant to ProJenX Inc, and serves as a consultant to Weatherwax Biotechnologies Corporation. K.S. serves on the scientific advisory board of FELIQS Corporation.

■ ACKNOWLEDGMENTS

We thank Dr. Brian Shoichet (University of California, San Francisco) for insightful discussions and guidance regarding the use of SEA in this study. This research was supported by the National Cancer Institute (P01CA291697), and a Cancer Center Support Grant (P30CA008748), and the Columbia University Digestive and Liver Disease Research Center (funded by NIH grant 5P30DK132710) through use of its Bioimaging Core, Bioinformatic and Single Cell Analysis Core, Organoid and Cell Culture Core and Clinical Biospecimen and Research Core, and the Cancer Center Flow Core Facility and Genomics and High Throughput Screening Shared Resource funded in part through the National Institutes of Health/National Cancer Institute Cancer Center Support Grant (P30CA013696), and P01AG002132 (to EGP). Artificial intelligence−based language tools were used for limited editorial assistance during manuscript preparation; all scientific content, analyses, and interpretations were determined by the authors.

■ ABBREVIATIONS USED

AUC, area under the curve; ΔAUC, change in area under the curve; SAR, structure−activity relationship; SEA, Similarity Ensemble Approach; TEA, Target Enrichment Analysis; ATOC, α-tocopherol; DMSO, dimethyl sulfoxide; ECFP4, extended-connectivity fingerprint (diameter 4)

■ REFERENCES

(1) Swinney, D. C. Phenotypic vs. Target-Based Drug Discovery for First-in-Class Medicines. *Clinical Pharmacology & Therapeutics* **2013**, *93* (4), 299−301.

(2) Hafner, M.; Mills, C. E.; Subramanian, K.; Chen, C.; Chung, M.; Boswell, S. A.; Everley, R. A.; Liu, C.; Walmsley, C. S.; Juric, D.; Sorger, P. K. Multiomics Profiling Establishes the Polypharmacology of FDA-Approved CDK4/6 Inhibitors and the Potential for Differential Clinical Activity. *Cell Chemical Biology* **2019**, *26* (8), 1067−1080.

(3) Hu, Y.; Jasial, S.; Bajorath, J. Promiscuity Progression of Bioactive Compounds over Time. *F1000Research* **2015**, *4*, 118.

(4) Dixon, S. J.; Lemberg, K. M.; Lamprecht, M. R.; Skouta, R.; Zaitsev, E. M.; Gleason, C. E.; Patel, D. N.; Bauer, A. J.; Cantley, A. M.; Yang, W. S.; Morrison, B.; Stockwell, B. R. Ferroptosis: An Iron-Dependent Form of Nonapoptotic Cell Death. *Cell* **2012**, *149* (5), 1060−1072.

(5) Shimada, K.; Skouta, R.; Kaplan, A.; Yang, W. S.; Hayano, M.; Dixon, S. J.; Brown, L. M.; Valenzuela, C. A.; Wolpaw, A. J.; Stockwell, B. R. Global Survey of Cell Death Mechanisms Reveals Metabolic Regulation of Ferroptosis. *Nat. Chem. Biol.* **2016**, *12* (7), 497−503.

(6) Soldi, R.; Horrigan, S. K.; Cholody, M. W.; Padia, J.; Sorna, V.; Bearss, J.; Gilcrease, G.; Bhalla, K.; Verma, A.; Vankayalapati, H.; Sharma, S. Design, Synthesis, and Biological Evaluation of a Series of

Anthracene-9,10-Dione Dioxime β-Catenin Pathway Inhibitors. *J. Med. Chem.* **2015**, *58* (15), 5854−5862.
(7) Ko, P.-J.; Woodrow, C.; Dubreuil, M. M.; Martin, B. R.; Skouta, R.; Bassik, M. C.; Dixon, S. J. A ZDHHC5-GOLGA7 Protein Acyltransferase Complex Promotes Nonapoptotic Cell Death. *Cell Chemical Biology* **2019**, *26* (12), 1716−1724.
(8) Kahlson, M. A.; Ritho, J.; Gomes, J. V.; Wang, H.; Butterwick, J. A.; Dixon, S. J. Functional Dissection of the zDHHC Palmitoyltransferase 5-Golgin A7 Palmitoylation Complex. *J. Biol. Chem.* **2025**, *301* (10), 110694.
(9) Leak, L.; Wang, Z.; Joseph, A. J.; Johnson, B.; Chan, A. A.; Decosto, C. M.; Magtanong, L.; Ko, P.-J.; Lee, W. C.; Ritho, J.; Manukian, S.; Millner, A.; Chitkara, S.; Salinas, J. J.; Skouta, R.; Rees, M. G.; Ronan, M. M.; Roth, J. A.; Myers, C. L.; Moffat, J.; Boone, C.; Bensinger, S. J.; Nathanson, D. A.; Atilla-Gokcumen, G. E.; Moding, E. J.; Dixon, S. J. Tegavivint Triggers TECR-Dependent Non-apoptotic Cancer Cell Death. *Nat. Chem. Biol.* **2025**, *21* (12), 1873−1884.
(10) Keiser, M. J.; Roth, B. L.; Armbruster, B. N.; Ernsberger, P.; Irwin, J. J.; Shoichet, B. K. Relating Protein Pharmacology by Ligand Chemistry. *Nat. Biotechnol.* **2007**, *25* (2), 197−206.
(11) Keiser, M. J.; Setola, V.; Irwin, J. J.; Laggner, C.; Abbas, A. I.; Hufeisen, S. J.; Jensen, N. H.; Kuijer, M. B.; Matos, R. C.; Tran, T. B.; Whaley, R.; Glennon, R. A.; Hert, J.; Thomas, K. L. H.; Edwards, D. D.; Shoichet, B. K.; Roth, B. L. Predicting New Molecular Targets for Known Drugs. *Nature* **2009**, *462* (7270), 175−181.
(12) Gregori-Puigjané, E.; Setola, V.; Hert, J.; Crews, B. A.; Irwin, J. J.; Lounkine, E.; Marnett, L.; Roth, B. L.; Shoichet, B. K. Identifying Mechanism-of-Action Targets for Drugs and Probes. *Proc. Natl. Acad. Sci. U.S.A.* **2012**, *109* (28), 11178−11183.
(13) Taylor, J. S.; Reid, T. S.; Terry, K. L.; Casey, P. J.; Beese, L. S. Structure of Mammalian Protein Geranylgeranyltransferase type-I. *EMBO J.* **2003**, *22* (22), 5963−5974.
(14) Zhang, F. L.; Moomaw, J. F.; Casey, P. J. Properties and Kinetic Mechanism of Recombinant Mammalian Protein Geranylgeranyltransferase Type I. *J. Biol. Chem.* **1994**, *269* (38), 23465−23470.
(15) Penning, T. M.; Wangtrakuldee, P.; Auchus, R. J. Structural and Functional Biology of Aldo-Keto Reductase Steroid-Transforming Enzymes. *Endocr Rev.* **2019**, *40* (2), 447−475.
(16) Reed, M. J.; Purohit, A.; Woo, L. W. L.; Newman, S. P.; Potter, B. V. L. Steroid Sulfatase: Molecular Biology, Regulation, and Inhibition. *Endocr Rev.* **2005**, *26* (2), 171−202.
(17) Hilborn, E.; Stål, O.; Jansson, A. Estrogen and Androgen-Converting Enzymes 17β-Hydroxysteroid Dehydrogenase and Their Involvement in Cancer: With a Special Focus on 17β-Hydroxysteroid Dehydrogenase Type 1, 2, and Breast Cancer. *Oncotarget* **2017**, *8* (18), 30552−30562.
(18) Dixon, S. J.; Patel, D. N.; Welsch, M.; Skouta, R.; Lee, E. D.; Hayano, M.; Thomas, A. G.; Gleason, C. E.; Tatonetti, N. P.; Slusher, B. S.; Stockwell, B. R. Pharmacological Inhibition of Cystine-Glutamate Exchange Induces Endoplasmic Reticulum Stress and Ferroptosis. *eLife* **2014**, *3*, No. e02523.
(19) Corbi, G.; Conti, V.; Russomanno, G.; Longobardi, G.; Furgi, G.; Filippelli, A.; Ferrara, N. Adrenergic Signaling and Oxidative Stress: A Role for Sirtuins? *Front. Physiol.* **2013**, *4*, 324.
(20) Lima, J. J.; Feng, H.; Duckworth, L.; Wang, J.; Sylvester, J. E.; Kissoon, N.; Garg, H. Association Analyses of Adrenergic Receptor Polymorphisms with Obesity and Metabolic Alterations. *Metabolism* **2007**, *56* (6), 757−765.
(21) Wang, B.; Tontonoz, P. Liver X Receptors in Lipid Signalling and Membrane Homeostasis. *Nat. Rev. Endocrinol* **2018**, *14* (8), 452−463.
(22) Chen, C.-H.; Budas, G. R.; Churchill, E. N.; Disatnik, M.-H.; Hurley, T. D.; Mochly-Rosen, D. Activation of Aldehyde Dehydrogenase-2 Reduces Ischemic Damage to the Heart. *Science* **2008**, *321* (5895), 1493−1495.
(23) Uchida, K.; Stadtman, E. R. Modification of Histidine Residues in Proteins by Reaction with 4-Hydroxynonenal. *Proc. Natl. Acad. Sci. U. S. A.* **1992**, *89* (10), 4544−4548.
(24) Gaulton, A.; Bellis, L. J.; Bento, A. P.; Chambers, J.; Davies, M.; Hersey, A.; Light, Y.; McGlinchey, S.; Michalovich, D.; Al-Lazikani, B.; Overington, J. P. ChEMBL: A Large-Scale Bioactivity Database for Drug Discovery. *Nucleic Acids Res.* **2012**, *40* (D1), D1100−D1107.
(25) Ward, J. H. Hierarchical Grouping to Optimize an Objective Function. *Journal of the American Statistical Association* **1963**, *58* (301), 236−244.
(26) Rogers, D.; Hahn, M. Extended-Connectivity Fingerprints. *J. Chem. Inf. Model.* **2010**, *50* (5), 742−754.
(27) Altschul, S. F.; Gish, W.; Miller, W.; Myers, E. W.; Lipman, D. J. Basic Local Alignment Search Tool. *J. Mol. Biol.* **1990**, *215* (3), 403−410.
(28) Korotkevich, G.; Sukhov, V.; Budin, N.; Shpak, B.; Artyomov, M. N.; Sergushichev, A. Fast Gene Set Enrichment Analysis. *bioRxiv* 2021; 060012.

https://doi.org/10.1021/acsmedchemlett.6c00020
ACS Med. Chem. Lett. XXXX, XXX, XXX−XXX